RSC Advances

ROYAL SOCIETY OF CHEMISTRY

www.rsc.org/advances

Cite this: DOI: 10.1039/c0xx00000x

www.rsc.org/xxxxxx

ARTICLE TYPE

One-step synthesis, characterization and catalytic performance of hierarchical Zn-ZSM-11 via facile ZnO routes

Qingjun Yu [a,b], Chunyi Li[*b] , Xiaolong Tang[a] and Honghong Yi[a]

Received (in XXX, XXX) Xth XXXXXXXXX 20XX, Accepted Xth XXXXXXXXX 20XX

DOI: 10.1039/b000000x

Hierarchical Zn-ZSM-11 zeolite with an olive-shaped intergrowth morphology was synthesized via a novel and facile one-step hydrothermal method by using tetrabutylammonium bromide (TBABr) and zinc oxide (ZnO) as a difunctional template and zinc source, respectively. Structural characterizations (XRD, IR, TG-DTA, SEM, and N_2 adsorption-desorption) were conducted to analyze the textural properties of Zn-ZSM-11 samples. Compared with the Zn containing ZSM-11 samples prepared by other methods ($ZnSO_4$ method, ZnO-impregnated-seed method and impregnation method), the Zn-ZSM-11 prepared by ZnO method exhibited enriched mesopores as well as good catalytic activity in methanol conversion. TEM images showed that Zn species were well incorporated into the zeolite framework, while the different morphology of Zn-ZSM-11 from ZSM-11 further verified that the Zn species had been involved in the formation of ZSM-11 framework. ^{27}Al and ^{29}Si MAS NMR spectra revealed that Zn species in zeolite framework significantly impacted the coordination of Si. The XRD patterns variation of the ZnO containing gel were also tracked to illustrate the crystallization process. It was found that the ZnO would be gradually dissolved under the severely alkaline environment and subsequently incorporated into the ZSM-11 framework in the crystallization process. This facile new synthesis strategy can also be extended to prepare other Zn containing zeolites and is potentially important for practical utilization.

1. Introduction

Over the last few decades, transition metal ions modified zeolites, particularly, the metal-modified pentasil zeolites have gained a great deal of attention since the incorporation of transition metals endows zeolites many special catalytic properties.[1-3] Among them, Zn or Ga modified ZSM-5 or ZSM-11 have been known as the active catalysts for aromatization of light paraffins;[4-6] the ZSM-5 and ZSM-11 zeolites containing Co or Cu display excellent activity in selective NO reduction with methane or NO and N_2O decomposition,[7-11] the modification of ZSM-5 zeolites with Fe and Mn confers to the materials a good selective oxidation performance.[12, 13] Generally, these metal species can be incorporated into the zeolite phase by post-treatment methods of ion-exchange or impregnation.[4, 14, 15] However, impregnation method often causes the aggregation of metal species, which might block the channels of zeolite. By contrast, the incorporated metal species via ion-exchange method have better dispersion in zeolite phase. Nevertheless, the post-treatment procedures make it complicated to obtain metal-zeolites materials and thus limit their industrial applications.

In view of this, the direct synthesis method of incorporating metal ions into the zeolite phase during the crystallization process seems to be a preferable way for its simplification to obtain well-dispersed and stable metal species in the zeolite framework.[1, 12, 16] In order to incorporate heteratoms into the zeolitic frameworks, some chemical factors must be considered. For example, the metal ion species should be able to undergo an easy mobilization in the gel phase, generally achieved through solubilization in basic (OH^-) or neutral (or acidic) (F^-) media. Then they also must be ready to condense further under the subsequent hydrothermal conditions.[17] However, most of the metal ions, like Fe^{3+} (Fe^{2+}), Cu^{2+}, etc., form more readily insoluble or sparingly soluble hydroxides or oxides that are hardly depolymerized and mobilized into the useful metallosilicate anionic species able to condense further viably to form zeolite framework. Thus, some specific synthetic conditions and a restricted selection of reactants are required to promote the incorporation of metals into zeolite framework. A few suitable mineralizing agents that can form metal complexes sufficiently stable as to prevent their progressive hydrolysis and their stepwise dissociation with the release of the metallic ionic species before their involvement in the zeolite crystallization process have been developed. Gabelica and Valange, in their review, have proposed that the short-chain alkylamine, as mobilizing-complexing agents, can effectively incorporate several metallic species (Zn^{2+}, Ga^{3+}, Fe^{3+}, Cu^{2+}, etc.) into the framework of ZSM-5.[17] Some other metallic precursors, such as manganese(III)-acetylacetonate,[12] $[Zn(NH_3)_4]^{2+}$ complex,[1, 16] were also prepared as one kind of reactant instead of being introduced in the form of metal salt. In addition, some researchers proposed that the metallic species could be introduced into the silica source. Then, the prepared metal-containing silica materials were mixed with the other materials of Al source,

NaOH and template. By this way, Fe-ZSM-5 with the morphology of nanorod-aggregation and poly-nanocrystallites has been obtained by Zhao [13] and Wang,[18] respectively.

In this paper, a very facile route was developed for the synthesis of ZnZSM-11 with a micropore-mesopore hierarchical structure by introducing ZnO directly into the silica-aluminum gel mixture with a pH of 12-13. It was found that the ZnO would be gradually dissolved and incorporated into the ZSM-11 framework with crystallization time under the severely alkaline environment. To the best of our knowledge, this is the first time that a highly Zn loaded ZSM-11 with hierarchical structure has been synthesized via a very facile route by adding ZnO into the reaction gel. For comparison, Zn was also introduced into the gel in the form of $ZnSO_4$ or ZnO-impregnated-seed. Besides, Zn containing ZSM-11 was also obtained by impregnation method to clarify the dispersion of Zn species in the zeolite crystals. In our previous study, it has been found that the hierarchical ZSM-11 with intergrowth morphology exhibit superior high selectivity to propylene as well as high gasoline yield in the methanol conversion reaction.[19] Here, the Zn containing ZSM-11 samples prepared by ZnO method were also applied in the methanol conversion and also present a good catalytic performance.

2. Experimental section

2.1 Materials

The synthesis was performed with colloidal silica (40 wt% SiO_2, 60 wt% H_2O, Qingdao Haiyang Chemical Co., Ltd.), aluminum sulfate ($Al_2(SO_4)_3 \cdot 18H_2O$, Sinopharm Chemical Reagent Co., Ltd.), sodium hydroxide (96.0 wt%, Sinopharm Chemical Reagent Co., Ltd.) as silica source, aluminum source and alkali source, respectively. Zinc oxide (ZnO, 99.7 wt%, Qingdao NakasenZinc& Technology Co., Ltd.), zinc sulfate ($ZnSO_4 \cdot 7H_2O$, 98.5 wt%, Sinopharm Chemical Reagent Co., Ltd.) and zinc nitrate ($Zn(NO_3)_2 \cdot 6H_2O$, 99 wt%, Sinopharm Chemical Reagent Co., Ltd.) were used as the Zinc source. Tetrabutylammonium bromide was used as the template to induce the structure of ZSM-11. All chemicals were used as received without further purification. Besides, hierarchical ZSM-11 with intergrowth morphology was chosen as seed crystals, which was prepared according to the literature.[20]

2.2 Synthesis of ZSM-11

The ZSM-11 without Zn species (Z11) was prepared as described as elsewhere.[21] In a typical synthesis, aluminum sulfate and sodium hydroxide were dissolved in deionized water, followed by addition of the mixture of silica sol and template (TBABr) (mixture I). Then, some amount of ZSM-11 seed crystals (5 wt% relative to the total solid content of the initial gel) were introduced. After vigorous stirring for a period, the well-mixed gel with the molar composition of 9.0 Na_2O: 1.0 Al_2O_3: 4ZnO: 65 SiO_2: 1.0 $(TBA)_2O$: 1300 H_2O was transferred to stainless-steel autoclaves, followed by a hydrothermal reaction at 170 ^oC for 12 h. After filtering, washing and drying at 100 ^oC, the obtained solid was calcined in air at 550 ^oC for 2 h to remove the template.

2.3 Synthesis of Zn-ZSM-11

Zn-ZSM-11 zeolites were obtained from the hierarchical ZSM-11 seeded gel mixture containing Zinc compounds via various synthesis methods.

(1) *Seed-$ZnSO_4$ method.* Zn-ZSM-11 zeolite synthesized by using zinc sulfate as zinc source was designated as Z11-Zn[S], which was prepared as follows: aluminum sulfate and sodium hydroxide were dissolved in deionized water, followed by addition of the mixture of silica sol and template (TBABr) (mixture I). Then, the aqueous solution of zinc sulfate was added dropwise into the former mixture I under strong stirring (mixture II). Finally, some amount of ZSM-11 seed crystals (5 wt% relative to the total solid content of the initial gel) was introduced to accelerate the crystallization process. After vigorous stirring for a period, the well-mixed gel was transferred to stainless-steel autoclaves, followed by a hydrothermal reaction at 170 ^oC for a period. After filtering, washing and drying at 100 ^oC, the obtained solid was calcined in air at 550 ^oC for 2 h to remove the template.

(2) *Seed-ZnO method.* The synthesis procedure as well as the reactant composition of sample Z11-Zn[O] was almost the same as that of Z11-Zn[S] except for the use of ZnO as zinc source. Instead of introducing the solution of $ZnSO_4$, the ZnO powder was added into the mixture II directly at a very slow rate.

(3) *ZnO-Impregnated seed method.* The extraneous seed was pretreated by the impregnation of zinc nitrate followed by the calcination to become the ZnO loaded form. For the synthesis of sample Z11-Zn[PreO], the Zn species was introduced into mixture II just in the form of ZnO loaded ZSM-11 seed.

All the initial gel mixture made by the three methods above have the same molar composition of 9.0 Na_2O: 1.0 Al_2O_3: 4.0 ZnO: 65 SiO_2: 1.0 $(TBA)_2O$: 1300 H_2O and the crystallization process were performed from 12 h to 36 h to get well-crystallized products. For comparison, all the products were obtained after crystallizing for 36 h.

(4) *Impregnation method.* For comparison, Zn-impregnated ZSM-11 sample was also prepared by the post-treatment method of impregnating an aqueous solution of $Zn(NO_3)_2 \cdot 6H_2O$ into the Z11 sample, followed by a calcination at 550 ^oC for 2 h. The resultant sample was designated as Z11-Zn[Pre].

2.4 Characterization

All samples were characterized by X-ray diffraction (XRD) on the X'Pert PRO MPD (PANalytical Co.) diffractometer at 40 kV and 40 mA with Cu Kα radiation at a scanning rate of 2 ^{o}/min in the 2 θ range from 4.5 to 65 ^{o}. The relative crystallinity was calculated based on the integration of the XRD characteristic peaks at 2 θ of 7.9 ^{o}, 8.7 ^{o}, 23.0 ^{o} and 23.9 ^{o} compared with that of the hierarchical ZSM-11 seed prepared according to literature.[20] The characteristic vibration bands of the zeolite particles were confirmed by FTIR on a Nexus Model Infrared Spectrophotometer (Nicolet Co, USA). Thermogravimetry (TG) and differential thermal analysis (DTA) were performed on a NETZSCH Proteus STA449C in an air stream at a programming rate of 10 ^oC/min from room temperature to 700^oC. Particle size and crystal morphology of the samples were examined with a scanning electron microscopy (SEM), S4800, equipped with an Energy dispersive X-ray spectroscopy (EDX) probe for the semi-

quantitative direct analysis of the elements. Nitrogen adsorption-desorption experiments at 77 K were conducted in an Autosorb instrument (Quantachrome).The total surface (S_{BET}) was calculated according to the (Brunauer-Emmet-Teller) BET isothermal equation, and the total volume (V_{total}) was determined from the nitrogen adsorbed volume at P/P_0=0.990. Both the micropore surface area (S_{micro}) and the micropore volume (V_{micro}) were calculated by application of the t-plot method. The external surface area (S_{ext}) and mesopore volume (V_{meso}) were obtained by the calculated total data minus the corresponding micropore data. Mesopore size distributions were obtained by using a method based on nonlocal density functional theory (NLDFT). The acid properties of samples were measured by pyridine adsorption on a Nexus Model Infrared Spectrophotometer (Nicolet Co, USA). X-ray fluorescence spectroscopy (XRF) conducted with an Axios Advanced X-ray Spectrometer was used to analyze the chemical compositions of samples. The transmission electron microscopy (TEM) images were recorded using a JEM-2100UHR transmission electron microscopy. UV-visible absorption spectra were measured on a JASCO V-550 UV-Vis spectrometer at room temperature. A Bruker AV-400 nuclear magnetic resonance (NMR) spectrometer was used to collect ^{27}Al and ^{29}Si MAS NMR spectra.

2.5 Catalytic performance

All the zeolites were transformed into the H-form by ion-exchanging Na-form with 1.0 M NH_4NO_3 solution at 80 ^oC for 2 h (three times), followed by washing, drying and calcination at 550 ^oC for 2 h. Then the H-form samples were used as an active component to be mixed intimately with silica sol and kaolin clay, which served as a binder and inert support for the zeolite, respectively. After stirring for 2 h, the formed slurry was dried at 100 ^oC for 3 h, followed by calcination at 700 ^oC for another 2 h. Then the catalyst bulks were crushed and sieved for later use.

The methanol-to-olefin (MTO) reaction was conducted to evaluate the catalytic performance of the Zn-ZSM-11 catalysts. For each test, 2 g catalyst with particle size of 0.250-0.425 mm was loaded between two layers of quartz wool in the reactor. After temperature got stable at 450 ^oC, the feed of pure methanol solution was introduced by a HPLC infusion pump at a fixed rate of 0.164 mL/min, accompanied with N_2 gas through a mass flow controller at a rate of 21 mL/min. The weight hourly space velocity (WHSV) for methanol was 5.53 h^{-1}. Effluent gas from the reactor was collected and analyzed by a Bruker 450-GC gas chromatography (GC) equipped with a TCD detector and a FID detector column. The corresponding liquid products were analyzed on Agilent 6820 gas chromatograph with an HP-INNOWAX capillarycolumn (30m×0.32mm×0.25μm) and a flame ionization detector (FID) using ethanol as internal standard. The coking amount was calculated from a TG-DTA curve measured on a NETZSCH Proteus STA449C in air at a heating rate of 10 ^oC/min from room temperature to 800 ^oC.

3. Results

Table 1 Textural properties of ZSM-11 and Zn-ZSM-11 samples prepared by various methods

	R.C., %		Particle size (μm) [c]	S_{micro} (m^2/g) [d]	S_{ext} (m^2/g) [e]	V_{micro} (cm^3/g) [f]	V_{meso} (cm^3/g) [g]
	XRD [a]	IR (I_{550}/I_{450}) [b]					
Z11	111.07	0.87	2.0-2.5	340.7	72.3	0.14	0.10
Z11-Zn[S]	64.78	0.84	Aggregation	220.4	24.3	0.09	0.04
Z11-Zn[O]	69.45	0.84	(1.5-1.7)*2.3	250.0	60.3	0.10	0.12
Z11-Zn[PreO]	76.11	0.82	(1.2-1.4)*1.7	242.5	50.2	0.10	0.09
Z11-Zn[Pre]	87.09	0.86	-	304.0	47.4	0.13	0.08

[a] The relative crystallinity was calculated based on the integration of the XRD characteristic peaks at 2 θ of 7.9 °, 8.7 °, 23.0 ° and 23.9 ° compared with that of the hierarchical ZSM-11 seed.

[b] The relative crystallinity estimated by the ratio of intensity of the band at 550 cm^{-1} and 450 cm^{-1} in the FTIR (fourier transform infrared spectroscopy) of samples.

[c] The particle size measured according to the SEM images of samples.

[d,f] Both the micropore surface area (S_{micro}) and the micropore volume (V_{micro}) were calculated by application of the t-plot method.

[e,g] Both the external surface area (S_{ext}) and mesopore volume (V_{meso}) were obtained by the calculated total data minus the corresponding micropore data, while the total surface (S_{BET}) was calculated according to the (Brunauer-Emmet-Teller) BET isothermal equation and the total volume (V_{total}) was determined from the nitrogen adsorbed volume at P/P_0=0.990.

XRD patterns

XRD was carried out to investigate the structure change of zeolite samples after zinc species were introduced via different methods. As shown in Figure 1(A), the diffraction patterns of the zinc containing samples are very similar with that of the blank sample Z11, all of which are belonged to the typical MEL topology. Besides, no diffraction peaks of ZnO crystallites are observed in the Zn-ZSM-11 samples, indicating that the zinc species are well dispersed in the zeolite crystals after they are introduced either via synthesis or impregnation methods. Notably, the Zn-ZSM-11 samples obtained from the direct synthesis of zinc contained gel mixtures also display an extra diffraction peak at about 2 θ of 5.96 °, which can be ascribed to carbonaceous organic species and can be removed by calcination in air flow (Figure 1A, inset).These results suggest that the existence of zinc species in the initial gel can react with the template to form organic species during the crystallization process, which might have an influence on the properties of final product zeolites.

Crystallinity, as assessed by both XRD and FTIR techniques, were listed in Table 1. When zinc species are introduced into the initial gel, the obtained Zn-ZSM-11 samples show evident decreased peak intensities than the Z11 sample, resulting in the very poor XRD crystilinity of Zn-contained samples. However, the ratios of optical densities of the 550 cm^{-1} band and 450 cm^{-1} band (I_{550}/I_{450}), which also can give an approximate estimation of the crystallinity for ZSM-11 or ZSM-5 zeolites,[4, 22] show no obvious difference among these Zn-ZSM-11 and ZSM-11 samples. As listed in Table 1, all the samples have the I_{550}/I_{450} ratio larger than 0.7, indicating that the crystallinity is approximate 100 %.[22, 23] These results indicate that the incorporation of Zn species has no obvious influence on the crystallization degree of zeolite structures but has an effect on the X-ray diffraction peak intensities of samples. It is well known that the XRD peak intensity can reflect the relative content of some phase in the whole samples. Therefore, it can be deduced that the decrease of peak intensity of Zn-ZSM-11 samples are probably due to the dilution of ZSM-11 phase by incorporating Zn species.

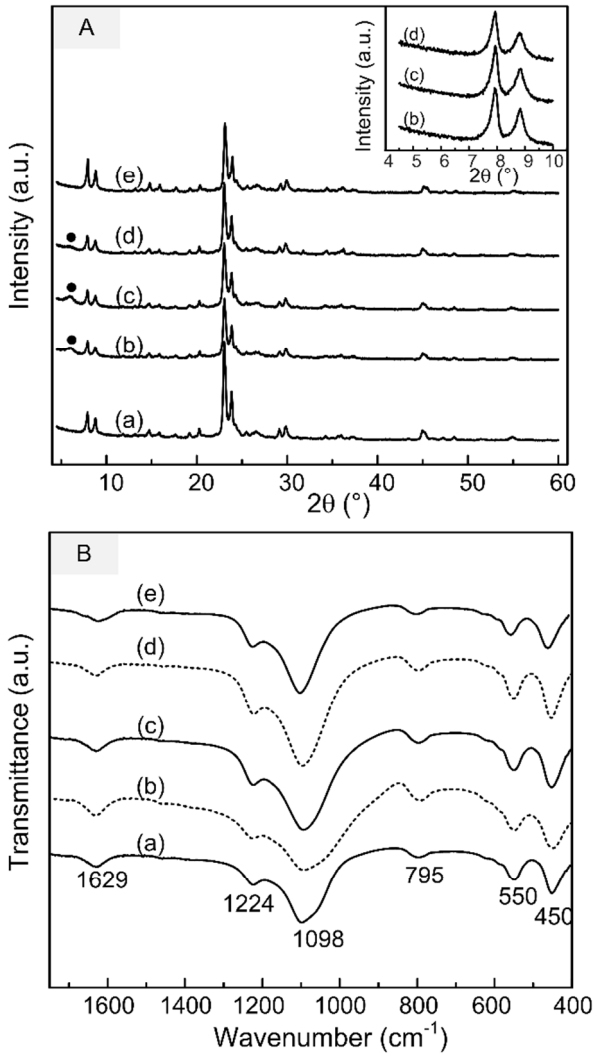

Fig.1 XRD patterns (A) and FTIR spectra (B) of Zn-ZSM-11 prepared by different methods: (a) Z11; (b) Z11-Zn[S]; (c) Z11-Zn[O]; (d) Z11-Zn[PreO]; (e) Z11-Zn[Pre]. The inset in Figure 1A is the enlarged 2θ region in 4-10 ° of XRD patterns of calcined samples (b), (c) and (d)

TG-DTA analysis

The TG-DTA analysis was carried out to determine the thermal stability of the synthesized ZSM-11 samples with or without Zn and to measure the weight loss of both water and templates. Thermograms of the samples were illustrated in Figure 2. Under air atmosphere, the main loss of weight for all the ZSM-11 samples with and without zinc occurs below 200 °C and in the range of 400-500 °C, which are caused by the loss of physically adsorbed water and the oxidative decomposition of the template present in zeolite channels, respectively.[24] It should be noted that all the Zn containing samples present an additional exothermic peak at 300-400 °C (Figure 2(b-d)), which cannot be observed in the ZSM-11 sample (Figure 2a). Considering the XRD peak at 2 θ of 5.96 °, it can be confirmed that the weight loss at 300-400 °C was due to the decomposition of carbonaceous organic species formed during the crystallization of zinc-containing gel mixture. In addition to the weight loss described above, there is no substantial weight loss above 500 °C in both Zn containing and blank ZSM-11 samples, indicating the Zn-containing ZSM-11 is as stable as the ZSM-11 material.

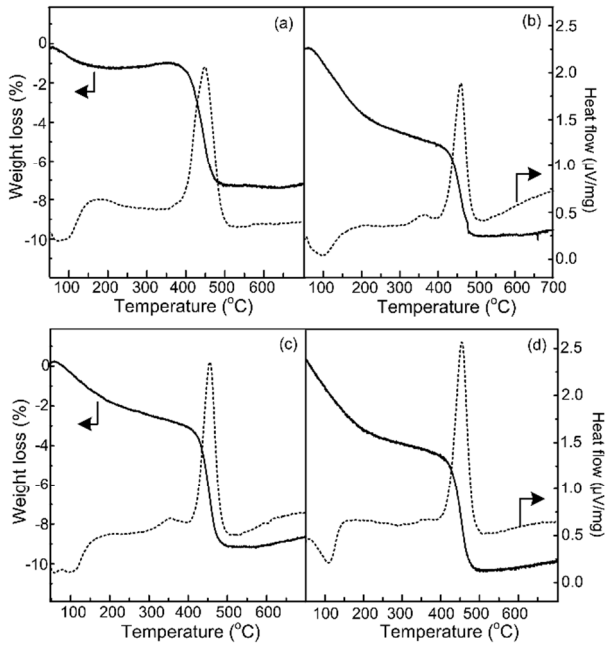

Fig.2 TG-DTA curves of ZSM-11and various Zn-ZSM-11 zeolites: (a) Z11; (b) Z11-Zn[S]; (c) Z11-Zn[O]; (d) Z11-Zn[PreO]

SEM images

SEM was used to understand the effect of zinc species on the morphology and crystal size distribution of ZSM-11 zeolites. Figure 3 shows SEM images of ZSM-11 and Zn-ZSM-11 synthesized by different methods. Intergrowth microsphere morphology of seed-assisted synthesized ZSM-11 is clearly observed and the particle size is about 2-3 μm (Figure 3b), much smaller than the extraneous hierarchical ZSM-11 microspheres (6-7 μm, Figure 3a). This distinction in particle size distribution of seed and product zeolites is mainly attributed to the surface nucleation behavior occurring on the seeds.[25] After zinc was

introduced into the initial gel, the prepared zinc containing products also exhibit the similar intergrowth morphology to Al-ZSM-11 (Figure S1), which is mainly due to the scaffold of TBABr for directing the meso-structure.[20, 26] Meanwhile, the size of individual particles for all the Zn-ZSM-11 samples is smaller than the seed's particle size, demonstrating that the incorporation of zinc species has no obvious effect on the behavior of seeds. Nevertheless, different from the microspherical nanorods aggregates of the pure ZSM-11, the zinc containing Zn-ZSM-11 samples display completely different particle shape, which vary with the synthesis methods. For instance, the sample Z11-Zn[S] prepared by seed-$ZnSO_4$ method have an irregular shape (Figure 3c), while the samples synthesized via Seed-ZnO and ZnO-Impregnated seed methods give uniform olivary (Figure 3d) and ellipsoidal shape (Figure 3e). The variation in shape of different zinc containing samples suggest that the existence of zinc species participate in the crystallization of MEL structure, irrespective of their various forms of ZnO or Zn-Al-Si species in the alkaline environment.

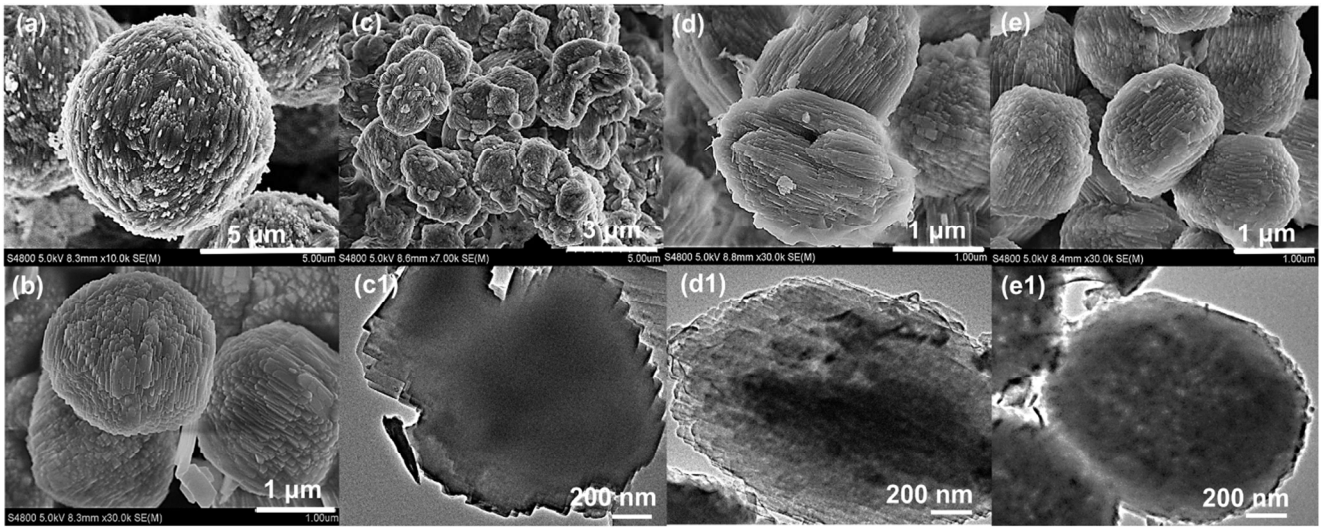

Fig.3 SEM images of ZSM-11and various Zn-ZSM-11 zeolites: (a) ZSM-11 seed; (b) Z11; (c) Z11-Zn[S]; (d) Z11-Zn[O]; (e) Z11-Zn[PreO] . (c1), (d1) and (e1) are the TEM images of an individual particle of sample Z11-Zn[S], Z11-Zn[O] and Z11-Zn[PreO]

N_2 isotherms

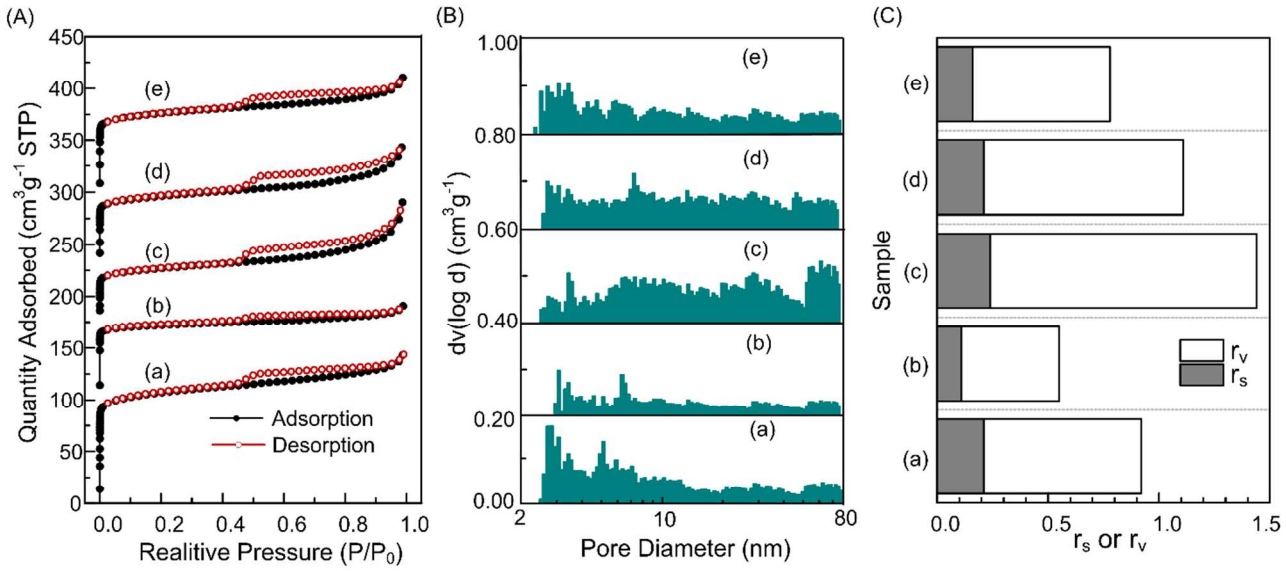

Fig.4 N_2 adsorption-desorption isotherms (A), the corresponding mesopore size distribution (DFT) (B) and the ratios of mesopore properties to micropore properties (C) of ZSM-11 and various Zn-ZSM-11 zeolites (r_s=external surface area/micropore surface area; r_v=mesopore volume/micropore volume)[27]: (a) Z11; (b) Z11-Zn[S]; (c) Z11-Zn[O]; (d) Z11-Zn[PreO]; (e) Z11-Zn[Pre]

The porosity properties of Zn-ZSM-11 samples were tested by nitrogen sorption experiments. Figure 4 (A) illustrates the N_2 adsorption-desorption isotherms of ZSM-11 and Zn-Al-ZSM-11 obtained by various methods. All the zinc containing materials show the similar isotherms to the blank sample Z11, which possess a steep increase at a low relative pressure of $10^{-7} < P/P_0 < 10^{-2}$ and a hysteresis loop at $P/P_0 = 0.4$-0.8, attributed to the filling of micropores and the capillary condensation of N_2 in mesopores,

respectively. What's more, a somewhat overlapping increase is also observed above $P/P_0 = 0.8$ in some samples and this is due to N_2 condensation in the larger voids between nanocrystals.[28, 29] The corresponding mesopore size distribution curves of various samples were depicted as Figure 4 (B). Compared with the blank ZSM-11 sample which mainly possesses the mesopore size distribution concentrated below 10 nm, the Zn containing samples show a wider size distribution ranging from 3 to 100 nm. Particularly, the sample Z11-Zn[O] prepared via the ZnO method shows an evident larger amount of pores with large size (> 50 nm) than the other samples (Figure 4B(c)), which is in good agreement with its larger N_2 adsorption amount in the higher pressure of $P/P_0 > 0.8$ (Figure 4A(c)). By contrast, the sample Z11-Zn[S] prepared by Seed-$ZnSO_4$ method shows the smallest mesoporsity, which is well agreement with the unconspicuous hysteresis loop of its isotherm. Considering the similar nanorods intergrowth morphology but different mesoporosity of these Zn containing samples, it is reasonable to deduce that the intergrowth or stacking state of the nanrod crystals in different samples varies with the preparation methods. Therefore, the voids that contribute greatly to the mesopore properties show great difference among different samples. TEM images were collected to illustrate the intergrowth of stacking state of nanoroods in various samples. As shown in Figure 3(d1, e1), dotted bright parts could be clearly observed among the intercrossed nanorod crystals of samples Z11-Zn[O] and Z11-Zn[PreO], demonstrating that the nanorods intergrowth or stack with each other in a relatively loose way. By contrast, the TEM image of sample Z11-Zn[S] present an almost whole dark microsphere (Figure 3c1), indicating that all the nanorod crystals intercrossed with each other in a close state. Correspondingly, the mesopore volume depended upon the voids existing among the aggregated nanorod crystals becomes the smallest in sample Z11-Zn[S].

Table 1 gives the detailed BET surface area and pore volume of the ZSM-11 materials with and without zinc species. When Zn species are introduced by impregnation method, a slight decrease is observed in both the micropore micropore surface and micropore volume due to the dilution effect. By contrast, the external surface area and mesopore volume show a greater decrease. The results reveal that the ZnO nanoparticles are mainly dispersed on the outer surface of the ZSM-11 crystals via impregnation followed by calcination. Compared with the sample Z11-Zn[Pre] obtained by impregnating Z11 with $Zn(NO_3)_2 \cdot 6H_2O$ followed by the calcination procedure, the samples synthesized directly from the zinc containing gel present obviously smaller micropore surface area (220-250 m^2/g) and volume (0.09-0.10 cm^3/g). Nevertheless, the Zn containing samples Z11-Zn[O] and Z11-Zn[PreO] show mesopore properties comparative to the Z11 sample. These results indicate that the Zn species are mainly incorporated into the micropore structures of samples through the direct synthesis method.

Generally, the existence of mesopore in microporous zeolite materials does a great contribution to improve the catalytic activity of materials due to the efficient mass transport.[20, 30] Here, the external to micropore surface area ratios (r_s) and the mesopore to micropore volume ratios (r_v) are used as practical parameters to characterize the mesoporosity of the samples. As shown in Figure 4 (C), it is evident to observe that the sample Z11-Zn[O], which incorporates Zn species in the form of ZnO, exhibits the largest mesopore properties, then followed by the sample Z11-Zn[PreO] prepared by the ZnO-impregnated-seed method. The sample Z11-Zn[Pre] prepared via the impregnation method presents a slightly decreased mesopore properties compared with the ZSM-11 zeolite (Z11), while the sample Z11-Zn[S] shows both the smallest r_s and r_v ratios, in accordance with its aggregation morphology. All these results above indicate that when Zn was introduced in the form of ZnO, these species can be well incorporated into the zeolite phase without affecting the formation of intercrystalline mesopores.

Acidity analysis

The FTIR spectra of pyridine adsorbed on ZSM-11 and Zn-ZSM-11 samples are shown in Figure 5. A serious of bands are observed over the blank ZSM-11 sample. According to the literature,[22, 31, 32] the bands at 1635 and 1540 cm^{-1} can be ascribed to the interaction of pyridine with Brønsted acid sites, while the bands at 1600 and 1450 cm^{-1} are due to the interaction of pyridine with Lewis acid sites. The band at 1490 cm^{-1} refers to the vibration of pyridine absorbed over Brønsted and Lewis acid sites. Notably, as zinc species are incorporated into the zeolite phase, the amount of Brönsted acid sites displays a significant decrease and the amount of Lewis acid sites increases. What's more, an additional intense signal at 1616 cm^{-1} is observed in all the ZnZSM-11 samples, representing the new Lewis acid sites generated by zinc incorporation.[33] Correspondingly, the band at 1450 cm^{-1} also splits into two bands after for the Zn-ZSM-11 samples. The position of the band at higher wavenumbers (1455 cm^{-1}) can be considered as the Lewis sites caused by Al species, while the band at lower wavenumbers (1440 cm^{-1}) can be assigned to the newly-formed Lewis sites. These results suggest the incorporation of Zn species can form more Lewis acid sites at the expense of consuming Brønsted sites. That is, the incorporated Zn species combine with the Brønsted acid sites and form the new [Al-O-Zn-O-Zn-O-Al] or [Al-O-Zn-O-Al] species, which act as the Lewis acid sites. [34, 35]

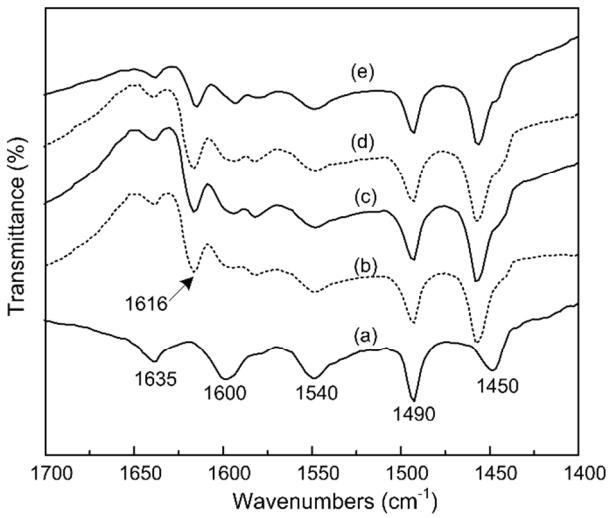

Fig.5 Py-IR spectra of ZSM-11 and Zn-ZSM-11 prepared by various methods: (a) Z11; (b) Z11-Zn[S]; (c) Z11-Zn[O]; (d) Z11-Zn[PreO]; (e) Z11-Zn[Pre]

Catalytic activity

The catalytic conversion of methanol was investigated over all the ZSM-11 catalysts with and without Zn species. As shown in Figure 6, these catalysts exhibit quite different catalytic activities. Compared with sample Z11, the Zn containing samples shows a relatively faster deactivation rate, which might be ascribed to the enhanced Lewis acid amount aroused by Zn species introduction. Among these Zn-ZSM-11 samples, when Zn species are introduced in the form of $ZnSO_4$, the obtained sample Z11-Zn[S] shows a rapid deactivation rate at the beginning of reaction. By contrast, the samples with the Zn species incorporated in the form of ZnO demonstrate a much slower deactivation rate and the deactivation rate decreases in the sequence of Z11-Zn[Pre] > Z11-Zn[PreO] > Z11-Zn[O]. Taking into account of the similar acidity but different textural properties among these Zn-ZSM-11 samples, it can be postulated that catalytic activity of various Zn-ZSM-11 samples greatly depends on their mesoporous properties. According to the report of Ryoo and coworkers, it was found that the coke was deposited on the external surfaces more than it was inside the micropores of ZSM-5 zeolites [36]. In this work, the intercrystalline voids among the nanorods of the Zn-ZSM-11 samples may act in a manner similar to the intracrystalline mesopores discussed by Ryoo and provide enough space to stock cokes and prevent the entrance of the micropore from blocking up [16]. Therefore, the Zn containing sample Z11-Zn[O], which possesses both largest r_s and r_v values, exhibits the longest catalytic lifetime, while the sample Z11-Zn[S] prepared by using $ZnSO_4$ method presents the lowest r_s and r_v values, resulting in its lowest catalytic activity.

It has been well documented that the Zn containing zeolites will yield more liquid products but less gaseous products than the H form zeolites.[16, 31] In this work, the gasoline yield variation with time on stream over different materials is depicted in Figure 6b. It is clearly observed that the Zn containing ZSM-11 samples show higher gasoline yield but a lower propylene selectivity than the Z11 sample after the reaction time of 90 min. Comparing the difference in acidity among these samples, it is rational to conclude that as the Zn species are incorporated into the ZSM-11 crystals, the decrease of Brønsted acid sites leads to the weaker propylene selectivity, while the increase of Lewis acid sites results in the increase of gasoline yield. In addition to the acidity, the textural properties of samples also play a vital role in the product selectivity. Obviously, the samples prepared via ZnO-seed methods still exhibit evident higher propylene selectivity than that prepared by impregnation method, following the order of Z11-Zn[O] > Z11-Zn[PreO] > Z11-Zn[Pre], which is corresponding to their different mesoporous properties (Figure 4C) [37].

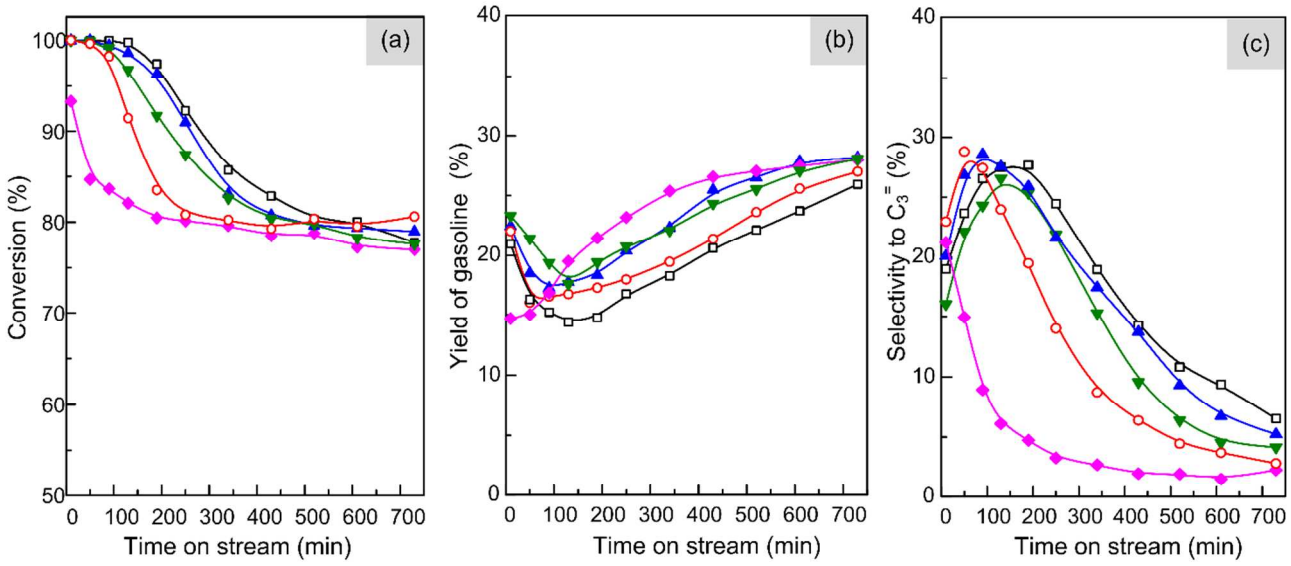

Fig.6 Catalytic performance in MTO over catalysts as a function of time on stream (□Z11; Z11-Zn[Pre]; Z11-Zn[O]; Z11-Zn[PreO]; Z11-Zn[S]).

4. Discussions

Table 2 Chemical composition of ZSM-11 and Zn-ZSM-11 prepared by different methods

Sample	Si/Al			Si/Zn		
	Initial mixture	EDX	XRF	Initial mixture	EDX	XRF
Z11	32.5	14.0	25.4	16.25	-	-
Z11-Zn[PreO]	32.5	13.0	26.4	16.25	7.9	25.3
Z11-Zn[O]	32.5	13.1	-	16.25	6.6	
Z11-Zn[S]	32.5	13.0	-	16.25	5.9	

Cite this: DOI: 10.1039/c0xx00000x

www.rsc.org/xxxxxx

ARTICLE TYPE

As described above, the incorporation ways of Zn species have a vital influence on the morphology and textural properties of the product samples, which finally affect their catalytic activity. The spherical intergrowth morphology is well retained when Zn species are introduced by impregnation method. No obvious ZnO clusters are observed in this sample, indicating that the Zn species are well dispersed in the crystals. In comparison, the Zn-ZSM-11 samples directly synthesized from the Zn containing gels show more or less different morphologies, revealing that Zn species have participated in the formation of ZSM-11 framework. In order to have a better comprehension on the behavior of Zn species in the synthesis process, the Si/Al and Si/Zn ratios were detected by both XRF and EDX. According to the surface analysis, the EDX is mainly used to carry out outer rim analysis, while the XRF can give the bulky composition.[4, 38]

For the sample ZSM-11, the aluminum near the surface (Si/Al=14.0 by EDX) is much higher than that in the whole crystal (Si/Al=25.4 by XRF). These results suggest that in the beginning of crystallization, silicon-rich nuclei are formed, while the aluminum species are primarily incorporated into the zeolite framework during the crystal growth process.[38-40] The similar case also appears when Zn species are introduced into the initial reaction gel. As listed in Table 2, the Zn containing sample Z11-Zn[PreO] shows a bulky Si/Zn ratio of 25.3, much larger than the outer rim Si/Zn ratio of 7.9, indicating that the Zn species are also incorporated in the crystal growth stage. It is noteworthy that all the three Zn containing samples present the similar Si/Al ratio (EDX) but different Si/Zn ratio. Considering their preparation methods, it can be reasonable to deduce that more amount of Zn species are incorporated into the framework when they are added in the form of Zn^{2+} than ZnO.

In the previous work, it has been found that the crystallization duration has a significant effect on the incorporation of aluminum species.[40] The longer period is needed for the completion of crystal growth, the more aluminum species will be incorporated into the framework and vice versa. Figure 7 gives the crystallization curves in different synthesis systems. Notably, when Zn is added into the gel mixture in the form of $ZnSO_4$, about 30 h is needed to get well crystallized product zeolites. For comparison, when Zn was introduced in the form of ZnO, the time necessary to complete the crystallization is much shorter. Particularly, in the system containing ZnO impregnated seed, the crystallization rate is as fast as that in the Zn-free system and only 6 h is needed to complete the crystallization process. Combining with the Si/Zn ratio of the three different samples, it is clear to find that the incorporation of Zn species also has a relationship with the crystallization duration. That is, more amount of Zn species will be incorporated into the zeolite phase after a longer crystallization period.

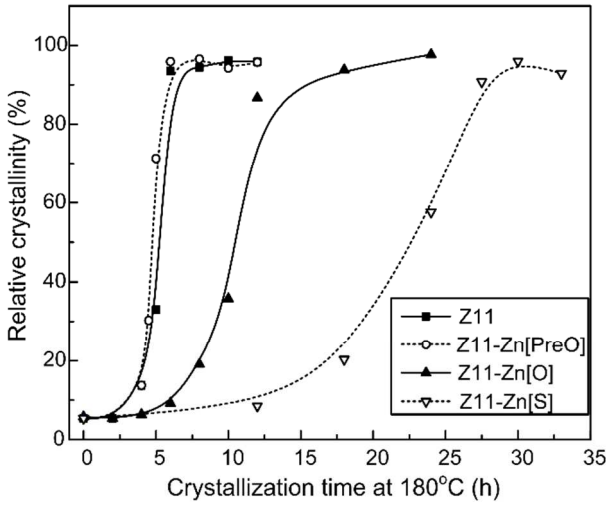

Fig.7 Crystallization curves of systems with and without Zn species by different methods

Cite this: DOI: 10.1039/c0xx00000x

www.rsc.org/xxxxxx

ARTICLE TYPE

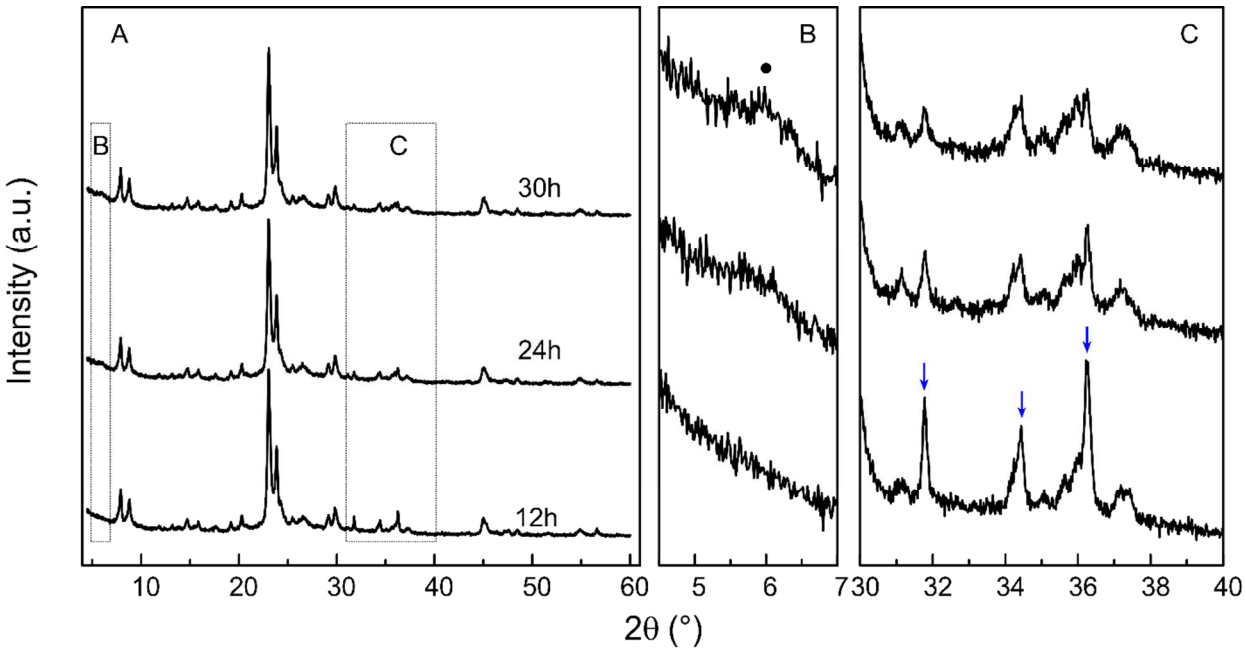

Fig.8 XRD peaks evolution of Z11-Zn[PreO] samples with crystallization time

It should be mentioned that in spite of the shortest time is needed to get well crystalline ZSM-11 phase when using ZnO impregnated seeds, the characteristic peaks designating ZnO clusters are also detected in the final products. As shown in Figure 8, the sample from the ZnO-impregnated-seed assisted system presents evident ZnO characteristic peaks even the crystallization time is prolonged to 12 h. As the hydrothermal crystallization time increases, the peak intensity representing the Zn content in the sample decreases and finally disappears at the crystallization time of 36 h. In the meantime, the diffraction peak at about 2 θ of 5.96 °, which designates the carbonaceous organic species appears. These results indicate the ZnO cluster can be dissolved in the alkaline environment at high temperature, irrespective of in a relatively long period. These soluble zinc species then will gradually participate in the crystallization of zeolite, which can be referred as the "recrystallization process". The formation of carbonaceous organic species verifies this recrystallization process.

Compared with the system containing ZnO-impregnated-seed, in the system where ZnO and seed are added into the system simutaneously, about twice time than the former (12 h) is needed to complete the crystallization process (Figure 9). But different from the former system, the ZnO peaks have disappeared after 10 h, at which time the ZSM-11 crystals are yet well crystallized. These results suggest that when Zn species are impregnated into the extraneous seed crystals before being added into the reactant gels, some interaction occurs between the ZnO clusters and seed crystal. Thus, the ZnO clusters cannot be easily dissolved in the presence of seeds and the Zn species are mainly incorporated into the zeolite phase in the subsequent recrystallization process.

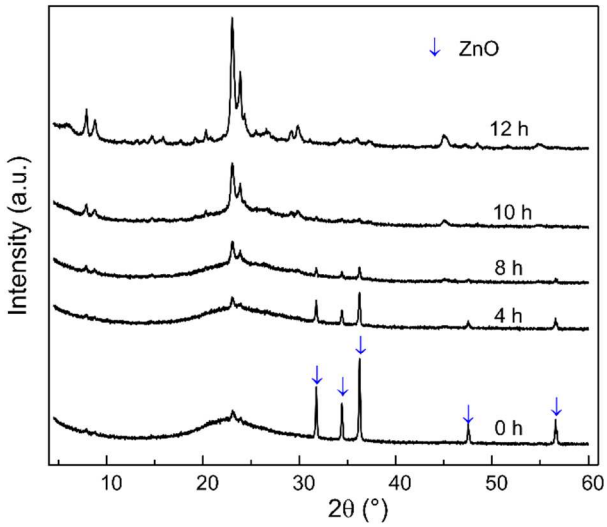

Fig.9 XRD peaks evolution of Z11-Zn[O] samples with crystallization time

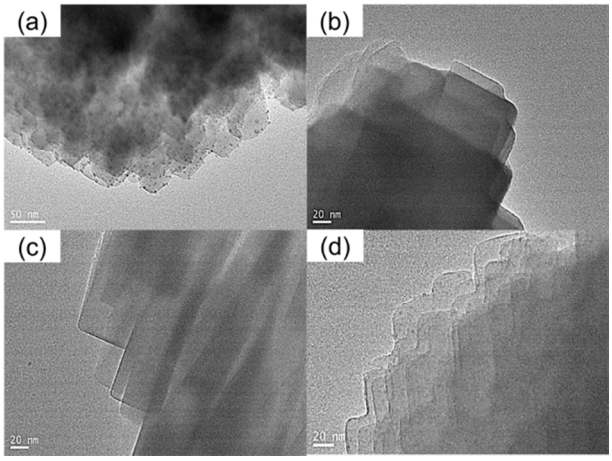

Fig.10 TEM images of Zn-ZSM-11 prepared by various methods: (a) Z11-Zn[Pre]; (b) Z11-Zn[S] (c) Z11-Zn[O] (d) Z11-Zn[PreO]

Theoretically, as the Zn species are incorporated as a counter ion, two Al are required in a nearly geometrical neighborhood to interact with one Zn^{2+}.[4] As a result, the theoretical Zn/Al value is about 0.5. In this paper, the product samples show the Zn/Al ratios of 1.6-2.2, much larger than the theoretical value (0.5). So it can be postulated that except for the Zn species incorporated into the zeolitic structures, there are still some Zn species existing in the ZSM-11 phase by dispersion or other forms. Figure 10 illustrates the state of Zn species in the ZSM-11 phase. From Figure 10a, obvious ZnO nanoparticles are observed in the zeolite crystals of sample obtained by impregnation method. By contrast, when Zn species are directly introduced as the reactant materials, no matter in the form of ZnO or Zn^{2+}, the crystallization product presents only zeolite phase, with no evident ZnO particles. From these results, it can be thought that the Zn species are well incorporated into the framework or well dispersed in the crystals through the direct synthesis method. Notably, if Zn species are impregnated into the seed crystal, the ZnO cannot be well involved in the formation of ZSM-11 frameworks. As shown in Figure 10d, evident ZnO particles can be observed in the crystal of sample Z11-Zn[PreO], however, in a much smaller amount than the impregnated sample Z11-Zn[Pre]. This result reveals that there are still some Zn species incorporated into the zeolitic structure during the crystallization process, which might mainly occur in the recrystallization stage.

^{27}Al and ^{29}Si MAS NMR have been viewed as a powerful characterization method to detect the coordination situation of Al and Si species in zeolite crystals, which can also reflect the state of Zn species in zeolite framework. Figure 11 shows the ^{27}Al and ^{29}Si NMR spectra of ZSM-11 and Zn-ZSM-11 samples prepared by various methods. All the samples exhibit one intense signal centered at around 54 ppm associated to tetrahedrally coordinated Al-atom in the framework,[41] indicating the introduction of Zn species has little effect on the incorporation of Al species into the frameworks. Nevertheless, the samples Z11-Zn[O] and Z11-Zn[S] prepared by adding ZnO or $ZnSO_4$ into the reaction gel display distinctively different ^{29}Si NMR spectra from the blank sample Z11. In addition to the four peaks in the range of -116~-103 ppm, which are assigned to the inequivalent framework T sites corresponding to Si(0Al) groupings (-112 and -116 ppm) [42] and Si(1Al) groupings (-107 and -103ppm), respectively,[41, 43, 44] another two evident signals are also observed below –100 ppm centered at -99 and -96 ppm, which can be attributed to Si(2Al) and Si(3Al) sites.[43] In contrary, the samples prepared by ZnO-impregnated-seed method only shows a very weak signal at -96 ppm, while the sample with Zn species introduced by impregnation method presents almost the same signals with the blank sample. These results further proved the postulation proposed above. That is, the Zn species can be well incorporated into the zeolitic framework to substitute the Si or Al sites through direct synthesis procedure. For the ZnO-Impregnated seed method, there will be two behaviors of Zn species in the crystals, some of them will be incorporated into the framework and the others will disperse in the crystals, which is similar to the impregnation method. What's more, from the difference of ^{27}Al and ^{29}Si NMR spectra among these samples with and without Zn, it is reasonable to believe that the incorporation of Zn species into zeolite framework has a close relationship with the Si species and thereby impact the coordination of Si species.

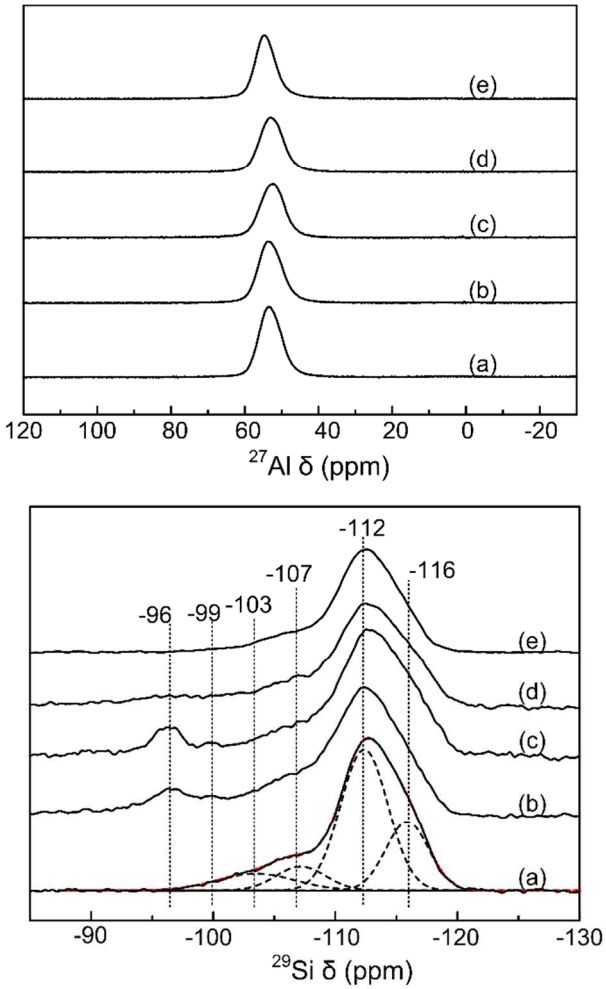

Fig.11 ^{27}Al MAS NMR and ^{29}Si MAS NMR spectra of Al-ZSM-11 and Zn-Al-ZSM-11 samples prepared by different methods. (a) Z11; (b) Z11-Zn[S]; (c) Z11-Zn[O]; (d) Z11-Zn[PreO]; (e) Z11-Zn[Pre]

Conclusions

In summary, we have developed a facile, one-step synthesis method to obtain hierarchical Zn-ZSM-11 with olive-shaped

intergrowth morphology and superior catalytic properties from the ZnO-containing gel mixture. For comparison, Zn containing ZSM-11 samples were also prepared by direct synthesis method of using $ZnSO_4$ or ZnO-impregnated-seed as zinc source and impregnation method. The XRD patterns and IR spectra shows that all the Zn containing samples possess pure ZSM-11 phase and high crystallinity. Besides, all the samples obtained from the direct synthesis method exhibit the similar intergrowth morphology to the extraneous seeds, which can be ascribed to the scaffold effect of TBABr. Nevertheless, the samples Z11-Zn[O], Z11-Zn[S] and Z11-Zn[PreO] exhibit obvious distinctive particle shape from the ZSM-11, indicating Zn species have been incorporated into the zeolite framework in the crystallization process and the incorporation amount follows the order of Z11-Zn[S] > Z11-Zn[O] > Z11-Zn[PreO]. The TEM images and ^{29}Si MAS NMR spectra further verify the fact that Zn species can be well incorporated into the ZSM-11 framework by ZnO and $ZnSO_4$ method, while only a small amount of Zn species can be incorporated into zeolitc framework by ZnO-impregnated seed method. Moreover, the ^{29}Si MAS NMR spectra also demonstrates that Zn species in the zeolite framework has an important impact the coordination of Si species. The textural properties determined by N_2 adsorption-desorption experiment shows that the sample Z11-Zn[O] prepared by ZnO method possesses both micropores and mesopores, further resulting in its good methanol converse activity. By tracking the crystallization process, it is found that the ZnO could be gradually dissolved under the severely alkaline environment and subsequently incorporated into the ZSM-11 framework during the crystallization process. However, in the ZnO-impregnated seeded system, the ZnO cannot be well incorporated in zeolite framework as a result of its interaction with seeds. This work provides a very simple route to synthesize Zn-ZSM-11 with good catalytic performance and this strategy can also be extended to prepare other Zn containing zeolites for reactions needing the Zn active sites and zeolite pore structures simultaneously.

Acknowledgements

This work is supported by the National 973 Program of China (No.2012CB215006). The authors also gratefully appreciate financial support from the special project on air pollution control of Beijing Municipal Science & Technology Commission (No.Z141100001014006).

Notes and references

[a] *Department of Environmental Engineering, Civil and Environmental Engineering School, University of Science and Technology Beijing, Beijing 100083,China;*
[b] *State Key Laboratory of Heavy Oil Processing, China University of Petroleum (East China), Qingdao 266555, China*

Corresponding author Fax: +86 532 86981787; Tel: +86 532 86981862; E-mail: chyli_upc@126.com; txiaolong@126.com

1. L. Wang, S. Sang, S. Meng, Y. Zhang, Y. Qi and Z. Liu, *Mater. Lett.*, 2007, **61**, 1675-1678.
2. J. Li, C. Hu, K. Tong, H. Xiang, Z. Zhu and Z. Hu, *RSC Adv.*, 2014, **4**, 44377-44385.
3. H. Chen, Y. Yan, Y. Shao and H. Zhang, *RSC Adv.*, 2014, **4**, 55202-55209.
4. O. A. Anunziata, J. Cussa and A. R. Beltramone, *Catal. Today*, 2011, 171, 36-42.
5. A. Hagen and F. Roessner, *Catal. Rev.*, 2000, **42**, 403-437.
6. J. A. Biscardi and E. Iglesia, *Catal. Today*, 1996, **31**, 207-231.
7. J. Armor, *Catal. Today*, 1995, **26**, 147-158.
8. M. Shelef, *Chem. Rev.*, 1995, **95**, 209-225.
9. M. Y. Kustova, A. Kustov, S. E. Christiansen, K. T. Leth, S. B. Rasmussen and C. H. Christensen, *Catal. Commun.*, 2006, **7**, 705-708.
10. M. Y. Kustova, S. B. Rasmussen, A. Kustov and C. H. Christensen, *Appl. Catal. B: Environ.*, 2006, **67**, 60-67.
11. P. Xie, Z. Ma, H. Zhou, C. Huang, Y. Yue, W. Shen, H. Xu, W. Hua and Z. Gao, *Microporous Mesoporous Mater.*, 2014, **191**, 112-117.
12. Y. Meng, H. C. Genuino, C.-H. Kuo, H. Huang, S.-Y. Chen, L. Zhang, A. Rossi and S. L. Suib, *J. Am. Chem. Soc.*, 2013, **135**, 8594-8605.
13. B. Li, B. Sun, X. Qian, W. Li, Z. Wu, Z. Sun, M. Qiao, M. Duke and D. Zhao, *J. Am. Chem. Soc.*, 2013, **135**, 1181-1184.
14. O. A. Anunziata, G. A. Eimer and L. B. Pierella, *Appl. Catal. A: Gen.*, 2000, **190**, 169-176.
15. L. Yu, S. Huang, S. Zhang, Z. Liu, W. Xin, S. Xie and L. Xu, *ACS Catal.*, 2012, **2**, 1203-1210.
16. Y. Ni, A. Sun, X. Wu, G. Hai, J. Hu, T. Li and G. Li, *Microporous Mesoporous Mater.*, 2011, **143**, 435-442.
17. Z. Gabelica and S. Valange, *Microporous Mesoporous Mater.*, 1999, **30**, 57-66.
18. J. Gu, Y. Jin, Y. Zhou, M. Zhang, Y. Wu and J. Wang, *J. Mater. Chem.A*, 2013, **1**, 2453-2460.
19. S. Wang, C. Li, X. Meng, Q. Yu, T. You, *CN 201210179763.8*, 2012.
20. Q. Yu, C. Cui, Q. Zhang, J. Chen, Y. Li, J. Sun, C. Li, Q. Cui, C. Yang and H. Shan, *J. Energy Chem.*, 2013, **22**, 761-768.
21. Q. Yu, J. Chen, Q. Zhang, C. Li and Q. Cui, *Mater. Lett.*, 2014, **120**, 97-100.
22. L. C. Lerici, M. S. Renzini, U. Sedran and L. B. Pierella, *Energ Fuel*, 2013, **27**, 2202-2208..
23. G. Coudurier, C. Naccache and J. C. Vedrine, *J. Chem. Soc., Chem. Commun.,* 1982, 1413-1415.
24. G. Wu, W. Wu, X. Wang, W. Zan, W. Wang and C. Li, *Microporous Mesoporous Mater.*, 2013, **180**, 187-195.
25. Q. Yu, Q. Zhang, J. Liu, C. Li and Q. Cui, *CrystEngComm*, 2013, **15**, 7680-7687.
26. J. Wang, J. C. Groen, W. Yue, W. Zhou and M. O. Coppens, *J. Mater. Chem.*, 2007, **18**, 468-474.
27. A. Gervasini, *Appl. Catal. A: Gen.*, 1999, **180**, 71-82.
28. R. Kore, R. Sridharkrishna and R. Srivastava, *RSC Adv*., 2013, **3**, 1317-1322.
29. H. Jin, M. B. Ansari and S.-E. Park, *Chem. Commun.*, 2011, **47**, 7482-7484.
30. Y. Tao, H. Kanoh, L. Abrams and K. Kaneko, *Chem. Rev.*, 2006, **106**, 896-910.
31. M. S. Renzini, U. Sedran and L. B. Pierella, *J. Anal. Appl. Pyrol.*, 2009, **86**, 215-220.
32. Y. Li, S. Liu, S. Xie and L. Xu, *Appl. Catal. A: Gen.,* 2009, **360**, 8-16.

33. O. A. Anunziata and L. B. Pierella, *Catal. Lett.*, 1993, **19**, 143-151.
34. J. A. Biscardi, G. D. Meitzner and E. Iglesia, *J. Catal.*, 1998, **179**, 192-202.
35. H. Berndt, G. Lietz and J. Völter, *Appl. Catal. A: Gen.*, 1996, **146**, 365-379.
36. J. Kim, M. Choi and R. Ryoo, *J. Catal.*, 2010, **269**, 219-228.
37. Mei, P. Wen, Z. Liu, H. Liu, Y. Wang, W. Yang, Z. Xie, W. Hua and Z. Gao, *J. Catal.*, 2008, **258**, 243-249.
38. Z. Gabelica, E. G. Deroune and N. Blom, ACS Publications, 1984, 219.
39. J. Martens and P. Jacobs, *Synthesis of high-silica aluminosilicate zeolites*, Elsevier, 1987.
40. Q. Yu, X. Meng, J. Liu, C. Li and Q. Cui, *Microporous and Mesoporous Materials*, 2013, **181**, 192-200.
41. N. Ren, Z. J. Yang, X. C. Lv, J. Shi, Y. H. Zhang and Y. Tang, *Microporous Mesoporous Mater.*, 2010, **131**, 103-114.
42. L. Zhang, S. Liu, S. Xie and L. Xu, *Microporous Mesoporous Mater.*, 2012, **147**, 117-126.
43. J. Dedecek, S. Sklenak, C. Li, B. Wichterlová, V. Gábová, J. i. Brus, M. Sierka and J. Sauer, *J. Phys. Chem. C*, 2009, **113**, 1447-1458.
44. J. P. Dong, J. Zou and Y. C. Long, *Microporous Mesoporous Mater.*, 2003, **57**, 9-19.

Graphic abstract for

One-step synthesis, characterization and catalytic performance of hierarchical Zn-ZSM-11 via facile ZnO routes

Qingjun Yu [a,b], Chunyi Li*[b], Xiaolong Tang*[a] and Honghong Yi[a]

[a] *Department of Environmental Engineering, Civil and Environmental Engineering School, University of Science and Technology Beijing, Beijing 100083,China;*

[b] *State Key Laboratory of Heavy Oil Processing, China University of Petroleum (East China), Qingdao 266555, China*

Corresponding author Fax: +86 532 86981787; Tel: +86 532 86981862; E-mail: chyli_upc@126.com; txiaolong@126.com

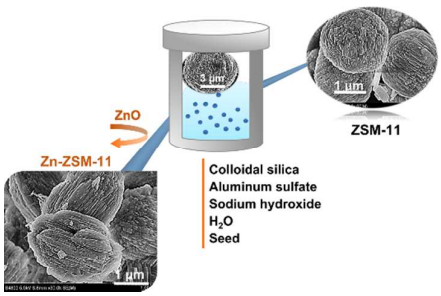

Hierarchical Zn-ZSM-11 with an olive-shaped intergrowth morphology was synthesized via a novel and facile one-step hydrothermal method.